Determination of displacement distributions in welded steel tension elements using digital image techniques

Sahin Sozen [*]

Department of Civil Engineering, Gaziosmanpasa University, 60200 Tokat, Turkey

Abstract.   It is known that material properties, connection quality and manufacturing methods are among the important factors directly affecting the behavior of steel connections and hence steel structures. The possible performance differences between a fabricated connection and its computer model may cause critical design problems for steel structures. Achieving a reliable design depends, however, on how accurately the material properties and relevant constitutive models are considered to characterize the behavior of structures. Conventionally, the stress and strain fields in structural steel connections are calculated using the finite elements method with assumed material properties and constitutive models. Because the conventional strain gages allow the measurement of deformation only at one point and direction for specific time duration, it is not possible to determine the general characteristics of stress-strain distributions in connections after the laboratory performance tests. In this study, a new method is introduced to measure displacement distribution of simple steel welded connections under tension tests. The method is based on analyzing digital images of connection specimens taken periodically during the laboratory tension test. By using this method, displacement distribution of steel connections can be calculated with an acceptable precision for the tested connections. Calculated displacements based on the digital image correlation method are compared with those calculated using the finite elements method.

Keywords: steel connections; digital image correlation; finite element analysis

1. Introduction

Digital image analysis and processing methods have found a broad range of applications in civil engineering disciplines since the enhancements of vision development systems and reduced hardware costs. One of the well-known applications in this field is the determination of deformations to characterize materials behavior under testing. Alternatively, deformation measurements have been used to identify relevant mechanical properties for constitutive models using function minimization procedures.

Strain measurement is very important for structural engineering. Electrical resistance strain gages are widely used to measure strains in testing of structural materials. While the use of strain gages is common due to their low cost and moderate instrumentation requirements, they offer, however, certain limitations depending on the environment temperature, material type, and

∗Corresponding author, Ph.D., E-mail: sahinsozen@gmail.com

measured strain magnitude. One of the common drawbacks in electrical resistance strain gages is that temperature change in the measurement environment generally introduces large errors to the measured strains due to non-linear response of the gage material. The usual practice is to apply a temperature compensation procedure in the measurement system to increase the reliability of measurements Beckwith *et al*. (2007). On the other hand, strain measurements under significantly lower or higher than the ambient temperature are generally costly and impractical. The type of materials used and the magnitude of measured strain also limit the performance of strain gages in typical measurement applications.

In recent years, an alternative method, digital image correlation (DIC), has been used by a number of researchers to determine material deformation and strain for which the typical strain gages are not suited in the case of discontinuous or large strain gradient zones Sutton *et al*. (1983). Digital image analysis and processing methods have also found a broad range of applications in civil engineering disciplines since the enhancements of vision development systems and reduced hardware costs. The DIC method can be successfully applied to study the behavior of various engineering materials under loading by measuring such as small strain contours for concrete and steel materials, or deformations of tunnel walls Choi and Shah (1997) and Wang *et al*. (2009). The use of DIC in fracture mechanics is also common; the method allows to study the stress intensity factor around a crack tip in static or dynamic loading conditions Chao *et al*. (1998), McNeill *et al*. (1987) and Yoneyama *et al*. (2006), and to monitor crack growth in fatigue tests Vanlanduit *et al*. (2009). Using high speed cameras, it is possible to study the materials behavior under dynamic loading which, in general, is a difficult application using conventional strain gages Jurjo *et al*. (2010). The DIC can be easily linked with the finite element method to validate the results of numerical solutions or compare between computed versus measured strains or displacements Pannier *et al*. (2006). Recent studies also show that the digital imaging techniques offer a great capability to structural engineers to monitor deformations, and study deformation characteristics of steel connections during the laboratory evaluation process De Roover *et al*. (2002), Spyrou and Davision (2001), Pan *et al*. (2012) and Pan and Li (2011). DIC method is used to design finite element model of the geomaterials Yue *et al*. (2003). The strength of structural materials such as concrete can be determined with the DIC method by combining conventional testing methods Başyiğit *et al*. (2012). The method can be easily used in non destructive testing Rathod *et al*. (2012). The method is widely used in other disciplines such as medicine application, agriculture application, traffic control etc. Swamy and Holi (2012), Iqbal *et al*. (2011), Zhang and He (2012), Wang *et al*. (2011), Yu *et al*. (2014) and Hassler *et al*. (2011).

The presented study in this paper introduces a simple laboratory test procedure to measure in-plane displacements in welded connections using digital image correlation method and compare with those calculated by the finite elements method. The method can easily be extended to calculate localized strains without having contact to the specimen surface under demanding measurement conditions.

2. Materials and method

The study was conducted using flat dogbone specimens, and three welded tension connection specimens subjected to the standard uniaxial tension loading. The specimens were fabricated from a flat steel sheet of 5 mm thickness, made of DIN EN 10025 S235JRG2 grade steel obtained from the Erdemir steel manufacturing company in Turkey. The selected material has a yield stress of

328 MPa, an ultimate strength of 427 MPa, and an ultimate strain of 44% according to the manufacturer's report.

2.1 Standard uniaxial tension specimens

Before analyzing the steel connections using the DIC method, three flat dogbone specimens were furnished with electrical resistance strain gages mounted on each specimen surface which have 120 Ohm gage resistance and 30 mm length and tested according to the ASTM A370-05 "*Standard Test Methods and Definitions for Mechanical Testing of Steel Products* specifications ASTM (2005). Strains at gage locations were then calculated using the DIC method and compared with the measured strains in order to verify the validity of the DIC method. The DIC results were found to be in good agreement with the measured strains for all the standard specimens. In Table 1, the strains computed at yielding using digital images are compared with the electrical resistance strain gage results. The last column displays the percent error in the image-based strains relative to the strain gage data. It can be seen that the image-based strains compare well with the measured (actual) strains with negligible errors given the order of magnitudes of the measured strains Sozen and Guler (2008, 2011). The yield stress and the ultimate stress of the material were measured as 328 MPa and 427 MPa, respectively from the standard tension tests. Standard test specimen is shown in Fig. 1. The narrowed section of the dogbone specimens was formed with a curvature having a radius of 13 mm. The specimen length and the width was adjusted by taking into account the maximum crosshead opening and the clamp width of the universal testing machine available in the test laboratory.

2.2 Welded steel connections

After the verification of the DIC method used, three simple welded tension connections were prepared for testing to determine the deformation fields using the DIC method. The connections were fabricated by utilizing two supplement plates on both faces of the connection using electrical corner welding of 3.5 mm thickness and 45 mm length. The relevant dimensions for the supplement plates and the connections can be observed from Fig. 2.

Because the grips of the testing equipment were only 50 mm in wide, special considerations were taken in the design of the test connections. Before the fabrication of actual specimens, two 3D finite element models of the connection were constructed in real dimensions with and without grip supporting end plates at specimen edges using the relevant material properties. The model was then subjected to an average tensile strain of 2% and solved for the longitudinal stress distribution and likely stress concentration locations that may cause early fracture of the test
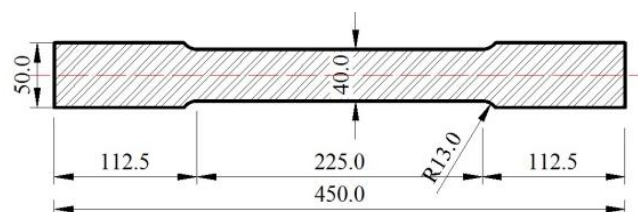

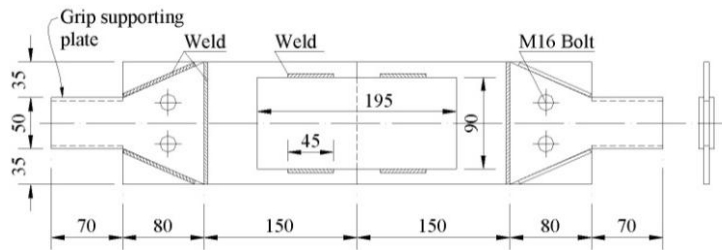Fig. 1 Standard dogbone specimen (dimensions are given in mm)

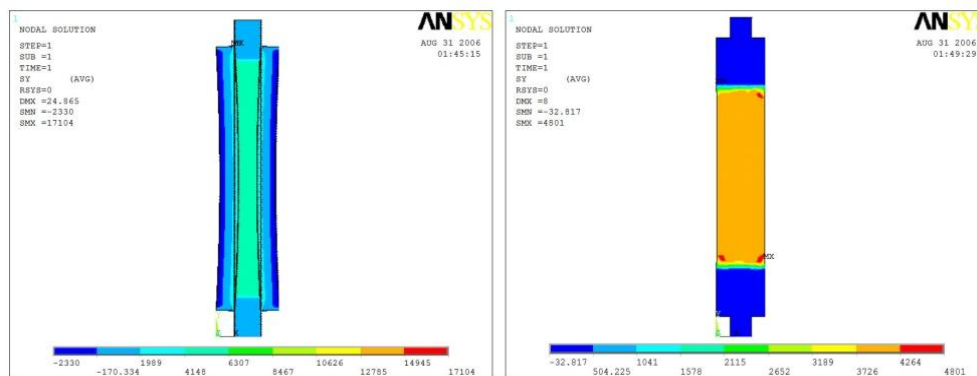Fig. 2 Specimen of welded tension element (dimensions are given in mm)

Fig. 3 Comparison of stress distribution based on finite element solution for standard steel specimens and specimens with grip supporting plates

specimen during testing. Fig. 3 shows the results of the finite element solution for the case of without grip supporting plate on the left, and with grip supporting plate on the right. The purpose of the supporting plates is to distribute the tension force applied on 50 mm wide edges to the entire cross section of the connection specimen. It can be seen that applying tension without the supporting plates cause non-uniform tensile stress hence deformation distribution throughout the cross section. The legends given in Fig. 3 represent the stress distributions in samples.

While the mid section is subjected to tensile stress, the specimen edges experience, however, substantial compressive stresses due to Poisson effect, which do not represent the expected behavior of a simple tension element. The results shown in Fig. 3 on the left indicated that in order to uniformly apply the tension load along the cross section, extra components must be designed for the end points of the connection. To achieve this, extra plates, gradually widening from 50 mm to 120 mm on the overlapped region were added to both sides of the specimen at the gripping location. As can be seen in Fig. 2. The plates were installed using electrical corner welding having a thickness of 3.5 mm and also strengthened using two M16 bolts of grade 8.8 to the main part in order not to allow collapse during tension test. All the connection components were welded according to the Manual (2002) and AWS (2006). The finite element solution with the supporting plates given in Fig. 3 indicated that stresses are uniformly distributed along the cross section with possible stress concentrations on the corner of supporting plates. Although the corners seemed to be potentially weak locations in which an early fracture in the main part may develop, the specimens with the supporting plates, however, all failed in the connection region showing no

effect of stress concentration on failure. Thus, extra supporting plates make it possible for the tension load to be distributed uniformly along the cross section if the tension can only be applied through a narrower grip section.

2.3 Specimen preparation for uniaxial tension tests

2.3.1 Preparation of standard test specimens

Preparation of standard specimens was achieved in two phases: generation of random speckle patterns on specimen surfaces, and installation of strain gages. In the first phase, random speckles were generated on one of the specimen surfaces from which the digital images were acquired. The random patterns are used in the cross-correlation function to calculate the displacement distribution between two sequential image frames Lecompte *et al*. (2007). Before this operation, sand blasting was applied on the specimens to obtain rust-free and smooth surfaces before the application of the speckle patterns. To generate random speckles, one of the specimen surfaces was first painted in white by a spray dye then black patterns were produced using a typical paint-brush. A picture of specimen with randomly generated speckle patterns can be seen in Fig. 4.

The first process was followed by the installation of strain gage on the specimen surface behind the speckle patterns so that the measured strain can be compared with the calculated strain around the same location using digital images. The selected gage length for the strain gages was 30 mm with a gage factor of 2.1. The installed strain gages were calibrated and connected to a USB based data acquisition system to obtain four readings per second. The data acquisition was performed by a user interface program that is coupled with the image acquisition system, so that the strain readings and image frames are acquired simultaneously at the same rate. A picture of a test

Fig. 4 Specimen with front surface with random speckle patterns (on top) and back surface (bottom) with strain gage installed
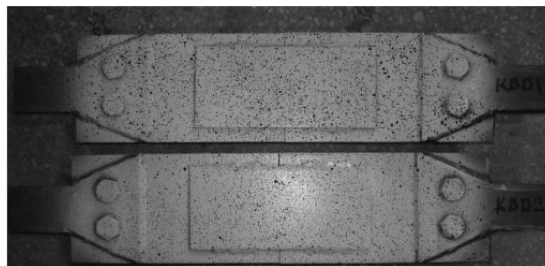

Fig. 5 A view of test specimen surface painted with random speckle patterns

Fig. 6 A view of test setup

specimen with strain gage installed can be seen in Fig. 4.

2.3.2 Preparation of welded steel connections

Preparation of welded connections for tension test is the same as preparation of standard tension specimens. Sand blasting was applied on specimens, one of the specimen surfaces was first painted in white by a spray dye then black patterns were produced. Strain gages were not used on welded connections.

A picture of specimen with randomly generated speckle patterns can be seen in Fig. 5. The test specimens were subjected to uniaxial tension tests according to the ASTM A370-05 procedures.

2.4 Uniaxial tension tests

The tests were conducted using a SATEC universal testing machine with a maximum tension capacity of 280 kN. The displacement rate was adjusted to 0.074 mm/s and kept constant throughout the test duration.

The test setup contained an image acquisition system, a USB data acquisition system, and a program with user-interface to control the test parameters and data recording. The image acquisition system included a Sony® XCD-X710 monochrome digital camera with a resolution of 1024×768 pixels, a C-mount lens with 12 mm fixed focal length, NI IEEE-1394 FireWire Driver/Board, and a fluorescent light source. After the specimen is mounted in the uniaxial testing machine, the camera setup is placed at a certain distance away such that the entire image area is used efficiently by the view of the test specimen. The image brightness, contrast and the light source position are all adjusted while the camera is set to the live mode. A view of the test setup can be seen in Fig. 6.

3. Computation of in-plane displacements from digital images

Digital image frames which have a resolution of 1024×768 pixels were captured at 1 frame per 2 seconds and saved onto the hard disk of a personal computer for further analysis. To calculate the strains from the digital pictures, displacement vector components need to be determined at the strain gage location mounted on the specimen surface. The average strain is then calculated from the displacement components and compared with the average strain measured using the electrical
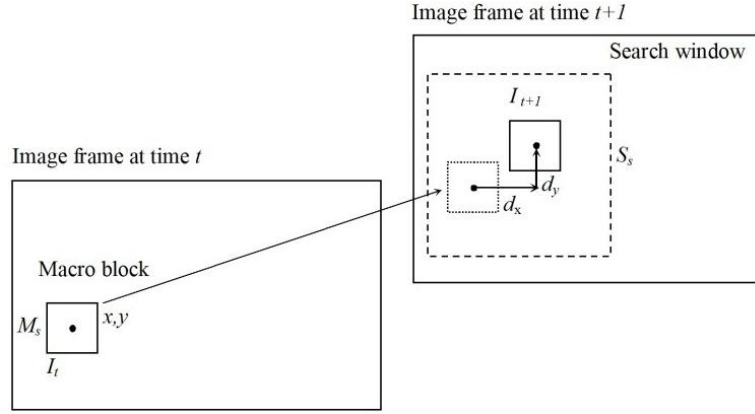
Fig. 7 Cross correlation between two sequential image frames

resistance strain gage installed on the specimen surface. The displacements are calculated in a two-component vector form (d_x, d_y) describing the motion of a rectangular pattern element called macro block. An image frame at time t is divided into a number of macro blocks and their matching patterns are searched for within the subsequent image frame at time $t + 1$ using the normalized cross-correlation algorithm given by The Math Works (URL 2009). The algorithm determines the components of a displacement vector describing the location of the best matching macro block within the frame at time $t + 1$, as illustrated in Fig. 7. This process is repeated for all the macro blocks constructed between the successive frames throughout the test duration.

Because the normalized-cross correlation is a computationally intensive process, the matching algorithm usually limits the search operation within a specific region called search window. The normalized cross-correlation can be given in Eq. 1 as follows

$$NCC(d_x, d_y) = \frac{\sum_{x,y} I_t(x, y) I_{t+1}(x + d_x, y + d_y)}{\sqrt{\sum_{x,y} I_t(x, y)^2 \sum_{x,y} I_{t+1}(x + d_x, y + d_y)^2}} \tag{1}$$

where NCC (d_x, d_y) = normalized cross correlation; $I_t(x, y)$ = pixel intensity at location (x, y) at time t; I_{t+1} ($x+d_x$, $y+d_y$) = pixel intensity at location ($x+d_x$, $y+d_y$) at time $t + 1$; and d_x, d_y = are the displacement components in x and y directions, respectively.

During the DIC analysis, the macro block size (M_s) and the search window size (S_s) are introduced into the algorithm by one of the dimensions of the defining rectangular area in units of pixels. The search window size is defined in relation to the macro block size and the displacement rate of testing. This is because of the fact that the maximum displacement that can be attained will be Max(d_x, d_y) = (S_s-M_s)/2 as the macro block is traveled within the search window. Consequently, an appropriate size of macro block and search window should be provided to the DIC analysis so that the displacement rate of testing does not cause an amount of displacement between the sequential frames that will exceed Max(d_x, d_y).

The macro block size depends, on the other hand, the characteristics of the speckle pattern generated within the digital frames, and capability of the DIC algorithm to calculate the displacement vectors. The macro block size needs to be adjusted in such a way that it should not cause excessive number of erroneous displacement vectors because of the poor matching between

the macro block pairs. The other parameter that is important for the macro block size relies on the capability of the implemented algorithm using whether rigid macro blocks or deformable macro blocks in the DIC analysis that can account for shearing, scaling and translation of macro blocks simultaneously. It can be normally expected that in the case of using rigid macro blocks the error in the calculated displacement vectors will increase if the in-plane deformations of the digital frames become significant. This means that the macro block size should be selected not too large to prevent the possible errors that will be introduced due to significant in-plane deformations exist in the image frames.

In the proposed DIC method, rigid macro blocks are assumed to calculate the displacement vectors using the normalized cross correlation function. Based on a number of trials, the optimal macro block size of 25×25 pixels was selected to minimize the number of erroneous displacement vectors and the effect of in-plane deformations of the captured frames. The search window size was selected as 35×35 pixels according to the rate of displacement of testing applied (0.074 mm/s), which accounts for a maximum displacement of 5 pixels between two sequential frames. After the DIC analysis, the calculated displacement vectors were used to determine the average strain at the strain gage location. Before the image acquisition process, the strain gage location was marked on the specimen surface, so that the macro blocks only within the specified region are used to calculate the average strain (see Fig. 8.) In addition, the time period for which the image frames are used to calculate the displacement vectors are determined from the strain gage data. The time at which the specimen is reached to the yielding was utilized to calculate the displacement vectors as shown in Fig. 9. This procedure was applied to all three test specimens to calculate the average strains from the digital images.
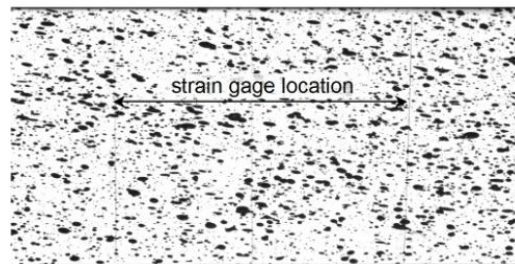

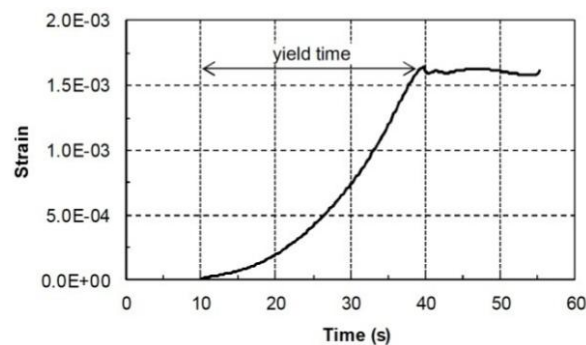Fig. 8 Image frame with a marked strain gage location

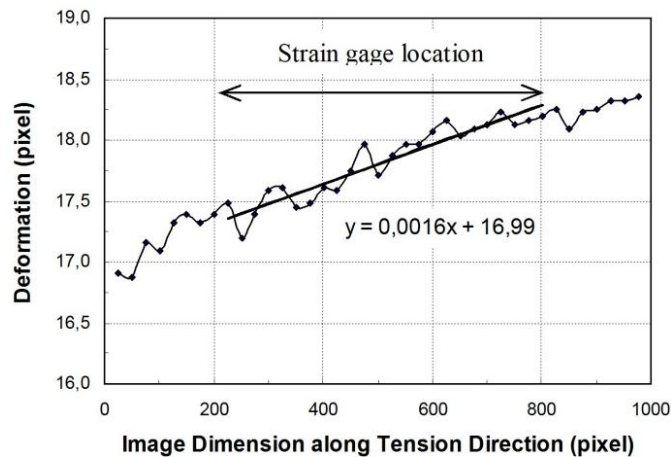Fig. 9 Strain gage data used to determine the yield time

Fig. 10 Average strain calculated from digital images at strain gage location

The average strain is calculated from the gradients of the displacement field within the strain gage location. The calculation procedure involves first plotting the horizontal components of the displacement vectors with respect to the image dimension along which the tensile stress is applied as shown in Fig. 10. The average strain is then obtained from the slope of a linear line fitted to the displacements at the strain gage location. The slope constant in the model gives the average strain calculated for the gage length of the strain gage up to the yield point. The intercept constant indicates the rigid body motion recorded in the captured frames during the tension test. Because the displacements are calculated using individual macro blocks along the tension direction, the trend shown in Fig. 10 exhibits some discontinuity that can be smoothed by an interpolation method if the strain at a specific point is to be estimated.

Using the displacement vectors at each macro block location, a contour map of the entire surface displacements can be determined. Using more sophisticated algorithms, it is also possible to calculate both in-plane principal strains and shear strains; however, this will be covered by the authors in future studies.

4. Finite element model of connection specimen

The finite element model of the welded connection was prepared as a 3D solid model using the commercial finite element software Ansys® as shown in Fig. 11. Solid element named Solid 95 of Ansys® was used in the model for steel and weld materials. Solid 95 has a quadratic displacement behavior and well suited to model irregular geometries. The element is defined by 20 nodes having three degrees of freedom at each node given in Ansys® Inc., Theory Manual (2010) A total of 6088 solid elements were used to construct the solid model of the tension connection specimen.

The finite element meshes were generated using two separate material models with different properties for steel and weld media. In addition, inelastic, isotropic and multi linear material solids were assumed in order to approximate the actual behavior of the model connection. For steel material, the assumed material properties are 300 MPa for the yield stress, and 400 MPa for the ultimate stress and 215 GPa for the Young's modulus. Similarly, according to the manufacturer's
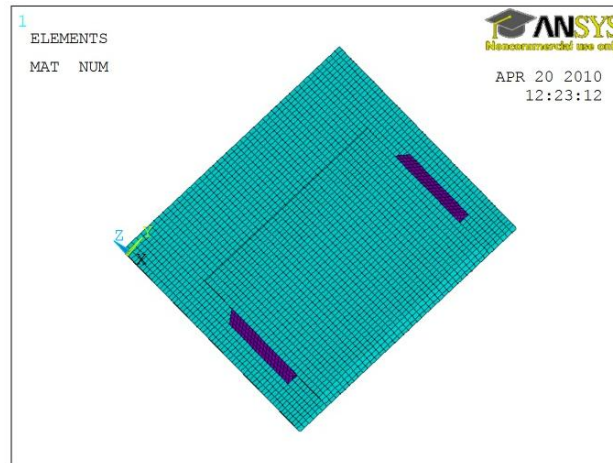
Fig. 11 Finite element model of the connection

record, 380 MPa and 600 MPa were assumed for the yield stress and the ultimate stress, respectively for the weld material. The Poisson's ratio is assigned as 0.3 for all the elements in the model. During the solution phase, ¼ part of the solid model was utilized by taking advantage of the symmetric form of the welded connection hence enhancing the computational performance and reducing the solution time in the analysis. The multi-linear stress-strain curve used in the finite element analysis can be seen in Fig. 12.

Inelastic, isotropic and multi-linear material model was assumed in order to approximate the actual behavior of the model connection. For the connection steel, the assumed material properties are: 300 MPa for the yield stress, 400 MPa for the ultimate stress, 215 GPa for the Young's modulus, and 0.3 for the Poisson's ratio.
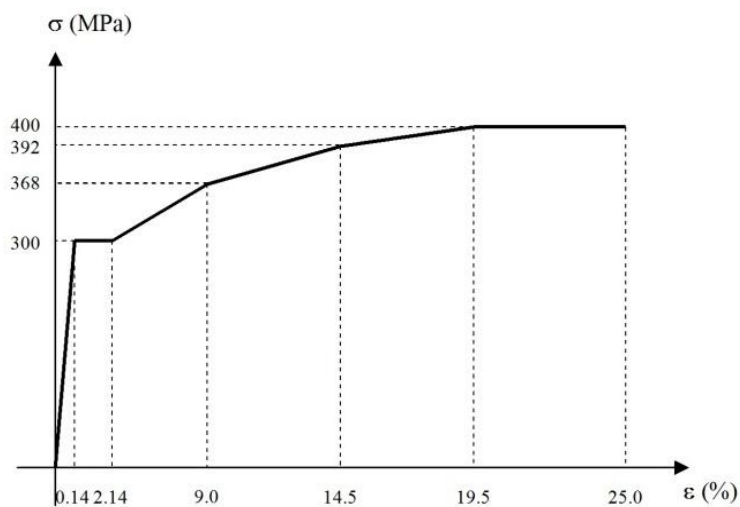

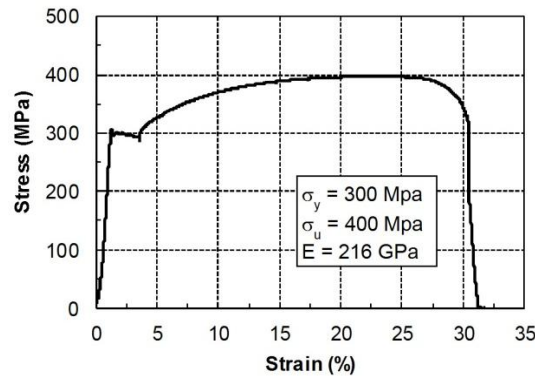Fig. 12 Stress-Strain curve for assumed connection materialsd

Fig. 13 Stress-strain curve for one of the standard specimens

Table 1 Comparison of yield strains measured by digital image correlation method and electrical resistance strain gages

Specimen	Strain gage (10^{-6})	Image frames (10^{-6})	Error (%)
1	1642	1626	0.98
2	1604	1627	1.40
3	1680	1616	3.83

5. Results and discussion

5.1 Test results for standard specimens

The results prove that the strains up to the yield point can be successfully measured by the DIC method, which can be an alternative tool for strain gages. One of stress-strain curves for the standard specimens is shown in Fig. 13. The yield stress, the ultimate stress and the elastic modulus of the steel material were measured as 300 MPa, 400 MPa and 216 GPa, respectively from the standard tension tests.

In Table 1, the strains computed at yielding using digital images are compared with the electrical resistance strain gage results. The last column displays the percent error in the image-based strains relative to the strain gage data. It can be seen that the image based strains compare well with the measured (actual) strains with negligible errors given the order of magnitudes of the measured strains. The results indicate that the amount of error produced is smaller than 5% for all the test specimens. It should be emphasized that the errors listed can be expected from temperature effects on strain gages, material non-linearity and macro block dimensions used in the matching algorithm.

5.2 Test results for connection specimens

Displacement fields for the steel welded connection specimen were determined using 3D finite element solid model using quadratic elements. The solution for the displacement component along the tension direction, e.g., UX direction in the finite element model, is shown in Fig. 14. The

model solution was carried out at the peak tension level of 185 kN measured during testing. In the displacement analysis using the DIC method, the strain level reached at this load level was used to determine the number of sequential frames for analysis. The displacement field measured using the DIC method is shown in Fig. 15 for one of the test specimens. The legends given in two figures represent the linear displacement along tension direction in mm. The solution from the finite element method indicates that a relatively constant displacement of around 1.4 mm takes place in the supplement plate while in the weld region the displacement changes from 0.15 mm to 1.09 mm because of highly non-linear stress localizations. The displacements on the main plate, on the other hand, seem to linearly increase from outer edge to the near weld region. It can be summarized that the displacement field within the connection region, in general, nearly constant on the supplement plate, linearly increasing from the edge to weld location, and highly non-linear in the weld region. The displacement field monitored in the DIC method is marked with dashed lines on the given
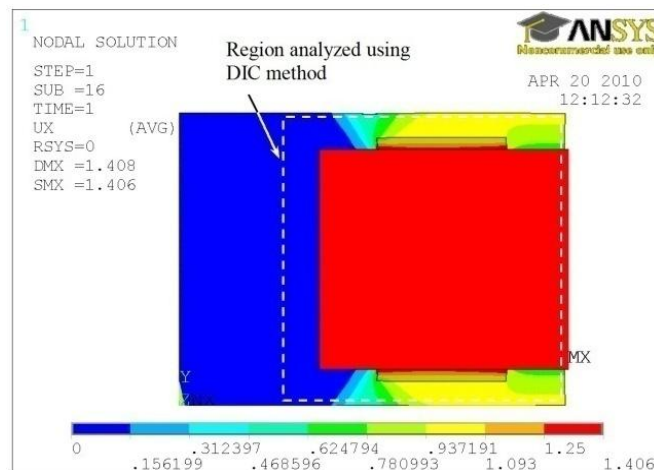

Fig. 14 Displacement distribution determined from the finite element model along with tension direction
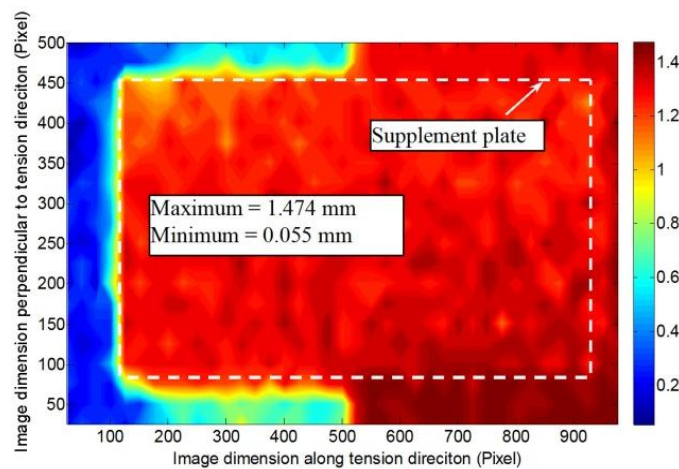

Fig. 15 Displacement distribution along with tension direction determined from DIC method

Table 2 Results of maximum and minimum displacements from DIC and finite element method

Specimen	DIC Method		Finite Element Method	
	Maximum displacement (mm)	Minimum displacement (mm)	Maximum displacement (mm)	Minimum displacement (mm)
1	1.474	0.055		
2	1.584	0.764	1.406	0.088
3	1.747	0.382		

graph in Fig. 14. The calculated displacement field using the DIC method for the same region is lso shown in Fig. 15. Comparison of the DIC results with those of Fig. 14 clearly shows that the actual displacement field is quite different from what is observed in the solid model. The measured maximum and minimum displacements from the DIC method were found to be 1.474 mm and 0.055 mm, respectively on the weld locations. The maximum displacement was measured on the right section of the connection while the minimum displacement seems to occur on left section. This clearly indicates that the failure started in the weld location on the right section hence the maximum displacement was reached during tension. Similar to the finding of the finite element solution, the supplement plate experienced nearly a rigid body motion showing minor changes in the displacement distributions.

It is believed that the difference between the displacement maps of the two methods is caused by the actual deformation behavior of the welds which could not be regarded in the finite element model. The weld material is assumed to be isotropic with a single modulus and Poisson ratio having a constant thickness and length in the solid model. In a fabricated connection, however, it is nearly impossible to achieve a welding with similar characteristics as assumed in the finite element model. It is because of this fact that one should expect relatively different displacement distributions hence strain and stress fields from the actual connection specimen and its solid model. For the differences between the measured and the calculated displacements using both methods, a similar statement can also be made because of possible defects that may exist in the steel material from which the main and the supplement plate was made.

The measured maximum and minimum displacements were also determined for the other two connection specimens and the results are listed in Table 2 together with those of finite element solution. It can be observed that the results from both methods seem to be close, however, their identified locations can be quite different because of possible defects in the welds, steel materials and nonlinearities, etc.

The use of DIC method offers several advantages when evaluating the performance of steel tension connections over the conventional methods: The DIC method allows engineers to justify the validity of the finite element solution and the material properties provided to the model. In this way, possible weakness of connection can easily be identified due to manufacturing defects in steel, poor workmanship in welding, and other reasons that cannot be accounted for in the finite element model. In addition, the method allows measurement of in-plane displacements on a localized basis or over a region of interest. Measurement can be achieved without any contact to the specimen surface, which provides flexibility in kind of applications where the measurement has be performed at certain proximity or under high temperature conditions in which conventional sensors may not be suitable.

6. Conclusions

In this study, digital image correlation method is introduced for measuring deformation as an alternative technique for conventional measurement procedures. The study was performed using three welded tension elements subjected to the standard tension tests. Deformations obtained from the DIC method are compared with those computed by finite elements solutions. The displacement field calculated from the finite element model can deviate significantly from the actual displacement field depending on the quality of materials used, and workmanship introduced during the fabrication of connections. The DIC method allows engineers to realistically evaluate the performance of connections that cannot be achieved through finite element modeling. The method offers several benefits over the conventional method for its practicality, instrumentation costs and applicability especially under demanding measurement conditions.

References

ASTM (2005), *A370-05*, Standard Test Methods and Definitions for Mechanical Testing of Steel Products, Society for Testing and Materials, USA.

AWS, D. (2006), D1. 1/D1. 1M-Structural Welding Code-Steel; American Welding Society, New York, NY, USA.

Başyiğit, C., Çomak, B., Kılınçarslan, Ş. and Serkan Üncü, İ. (2012), "Assessment of concrete compressive by image processing technique", *Construct. Build. Mater.*, **37**, 526-532.

Beckwith, T.G., Marangoni, R.D. and Lienhard, J.H. (2007), *Mechanical Measurements*, (6th Edition), Prentice Hall, NJ, USA.

Chao, Y.J., Luo, P.F. and Kalthoff, J.F. (1998), "An experimental study of the deformation fields around a propagating crack tip", *Exp. Mech.*, **38**(2), 79-85.

Choi, S. and Shah, S.P. (1997), "Measurement of deformations on concrete subjected to compression using image correlation", *Exp. Mech.*, **37**(3), 307-313.

De Roover, C., Vantomme, J., Wastiels, J. and Taerwe, L. (2002), "Deformation analysis of a modular connection system by digital image correlation", *Exp. Techniques*, **26**(6), 37-40.

Hassler, U., Rehak, M. and Ezrt, F. (2011), "An image processing approach for radioscopic inspection of turbine blades", *Proceedigs of International Symposium on Digital Industrial Radiology and Computed Tomography*, Fuerth, Germany, June.

Iqbal, S.M., Gopal, A. and Sarma, A.S.V. (2011), "Volume estimation of apple fruits using image processing", In: *Image Information Processing* (*ICIIP*), *Proceedings of 2011 International Conference on IEEE*, Himcahal Pradash, India, November, (pp. 1-6).

Jurjo, D.L.B.R., Magluta, C., Roitman, N. and Gonçalves, P.B. (2010), "Experimental methodology for the dynamic analysis of slender structures based on digital image processing techniques", *Mech. Syst. Signal Process.*, **24**(5), 1369-1382.

Lecompte, D., Bossuyt, S., Cooreman, S., Sol, H. and Vantomme, J. (2007), "Study and generation of optimal speckle patterns for DIC", *Proceedings of the Annual Conference and Exposition on Experimental and Applied Mechanics*, Costa Mesa, CA, USA, June.

Manual, C.F.S.D. (2002), *American Iron and Steel Institute*, Washington, D.C., USA.

McNeill, S.R., Peters, W.H. and Sutton, M.A. (1987), "Estimation of stress intensity factor by digital image correlation", *Eng. Fract. Mech.*, **28**(1), 101-112.

Pan, B. and Li, K. (2011), "A fast digital image correlation method for deformation measurement", *Optic. Laser. Eng.*, **49**(7), 841-847.

Pan, B., Dafang, W. and Yong, X. (2012), "Incremental calculation for large deformation measurement using reliability-guided digital image correlation", *Optic. Laser. Eng.*, **50**(4), 586-592.

Pannier, Y., Avril, S., Rotinat, R. and Pierron, F. (2006), "Identification of elasto-plastic constitutive parameters from statically undetermined tests using the virtual fields method", *Exp. Mech.*, **46**(6), 735-755.

Rathod, V.R., Anand, R.S. and Ashok, A. (2012), "Comparative analysis of NDE techniques with image processing", *Nondestruct. Test. Eva.*, **27**(4), 305-326.

Sozen, S. and Guler, M. (2008), "Measurement of Small Strains in Steel Samples Using Digital Imaging Technigues", *Proceedings of the 8th International Congress on Advances in Civil Engineering*, Famagusta, North Cyprus, September.

Sozen, S. and Guler, M. (2011), "Determination of displacement distributions in bolted steel tension elements using digital image techniques", *Optic. Laser. Eng.*, **49**,1428-1435.

Spyrou, S. and Davison, J.B. (2001), "Displacement measurement in studies of steel T-stub connections", *J. Construct. Steel Res.*, **57**(6), 649-661.

Sutton, M.A., Wolters, W.J., Peters, W.H., Ranson, W.F. and McNeill, S.R. (1983), "Determination of displacements using an improved digital correlation method", *Image Vision Comput.*, **1**(3), 133-139.

Swamy, M.S. and Holi, M.S. (2012), "Knee joint articular cartilage segmentation, visualization and quantification using image processing techniques: A review", *Int. J. Comput. Appl.*, **42**, 36-43.

URL (2010), http://www.ansys.com

URL (2009), http://www.mathworks.com

Vanlanduit, S., Vanherzeele, J., Longo, R. and Guillaume, P. (2009), "A digital image correlation method for fatigue test experiments", *Optic. Laser. Eng.*, **47**(3), 371-378.

Wang, T.T., Jaw, J.J., Chang, Y.H. and Jeng, F.S. (2009), "Application and validation of profile-image method for measuring deformation of tunnel wall", *Tunn. Undergr. Space Technol.*, **24**(2), 136-147.

Wang, Z.B., Yu, Z., Li, X.Y. and Luo, D.H. (2011), "A method of parameters estimation for traffic accidents by image and video processing", *Int. J. Video Image Process. Network Secur.*, **11**(6), 13-16.

Yoneyama, S., Morimoto, Y. and Takashi, M. (2006), "Automatic evaluation of mixed-mode stress intensity factors utilizing digital image correlation", *Strain*, **42**(1), 21-29.

Yu, Q., Zhu, W., Tang, C. and Yang, T. (2014), "Impact of rock microstructures on failure processes - Numerical study based on DIP Technique", *Geomech. Eng., Int. J.*, **7**(4), 375-401.

Yue, Z.Q., Chen, S. and Tham, L.G. (2003), "Finite element modeling of geomaterials using digital image processing", *Comput. Geotech.*, **30**(5), 375-397.

Zhang, R. and He, L. (2012), "Measurement of mixed-mode stress intensity factors using digital image correlation method", *Optic. Laser. Eng.*, **50**(7), 1001-1007.

CC